remote sensing

MDPI

Article

GPS/BDS Medium/Long-Range RTK Constrained with Tropospheric Delay Parameters from NWP Model

Ying Xu [1,*], Chen Wu [2], Lei Li [1], Lizi Yan [1], Min Liu [3] and Shengli Wang [4]

[1] College of Geomatics, Shandong University of Science and Technology, Qingdao 266590, China; xrzhmm@163.com (L.L.); ylz_email@163.com (L.Y.)
[2] Department of Land Surveying and Geoinformatics, The Hong Kong Polytechnic University, Hong Kong, China; wu.chen@polyu.edu.hk
[3] Shanghai Meteorological Bureau, Shanghai 200030, China; lisa8204@hotmail.com
[4] Institute of Ocean Engineering, Shandong University of Science and Technology, Qingdao 266590, China; shlwang@sdust.edu.cn
* Correspondence: yingxu@sdust.edu.cn; Tel.: +86-178-5326-7867

Received: 27 May 2018; Accepted: 9 July 2018; Published: 12 July 2018

Abstract: Tropospheric delay is a major error source that affects the performance of the Global Navigation Satellite Systems (GNSS) Real Time Kinematic (RTK) positioning especially for the medium/long-range baseline. Although high precision tropospheric delay can be estimated by GNSS carrier phase measurement, together with position and ambiguity, a relatively long period of convergence time is necessary. In this study, we develop a new GPS/BDS RTK algorithm constrained with a tropospheric delay parameters from Numerical weather prediction (NWP) model for medium/long-range baselines. The accuracy of the tropospheric delays derived from NWP is assessed through comparisons with the results of GAMIT (GNSS at MIT). The positioning performance with standard GPS RTK, standard GPS/BDS RTK, the developed NWP-constrained GPS RTK and NWP-constrained GPS/BDS RTK over medium/long-range baselines are compared in terms of the initialization time and the positioning accuracy. Experiment results show that the mean differences between the NWP and GAMIT zenith tropospheric delay (ZTD) are between −5.50 mm and 5.60 mm, and the RMS values of the NWP ZTD residuals are from 24.02 mm to 32.62 mm. A reduction in the initialization time of over 41% and 58% for medium- and long-range baselines can be achieved with the NWP-constrained RTK (both GPS alone and GPS/BDS RTK solutions) compared to the standard RTK solution, respectively. An improvement of over 30% can be found with the GPS/BDS RTK compared with that of the GPS alone RTK for both standard and the NWP-constrained modes. The positioning precision of NWP-constrained GPS/BDS RTK is better than 3 cm in the horizontal direction and better than 5 cm in the vertical direction, which satisfies the requirement of the precise positioning service.

Keywords: GPS/BDS; RTK; tropospheric delay; NWP model; medium/long-range baseline

1. Introduction

Real Time Kinematic (RTK) positioning with instantaneous ambiguity resolution (AR) and Precise Point Positioning (PPP) are currently popular techniques for real-time precise positioning based on carrier phase observation. These techniques have been widely used in surveying and navigation fields. A reliable real-time PPP service can provide precise positioning on a global scale [1]. However, PPP needs a comparatively long initialization time of about 20 min [2]. Generally, RTK provides centimeter-level positioning services with a relatively short initialization time over a baseline shorter

than about 80 km [3]. However, the GPS alone RTK shows limitations in the initialization time, convergence speed and positioning accuracy due to the insufficient visible satellite and limited spatial geometry, especially in urban areas where the signals are blocked or interrupted. In addition, RTK is limited to the local or regional area due to the significant ionospheric delay and tropospheric delay, especially over the medium/long-range baselines.

Global Navigation Satellite Systems (GNSS) are evolving to a new era due to the modernization of the current GPS and the upcoming other systems. The US GPS system achieved its Full Operation Capacity (FOC) in 1995 and is currently improving through the GPS modernization programme [4]. China started constructing its own satellite navigation system in the 1980s, called BeiDou Navigation Satellite System (BDS). The first generation of BDS (BDS-1) started service from 2003 with two Geostationary Earth Orbit satellites (GEOs). The service area covered China and the surrounding region with functions of positioning, timing and short message communication. The positioning accuracy of BDS-1 is better than 20 m. At the end of 2012, BDS-2 started service with 14 satellites, including five GEOs, five Inclined Geosynchronous Satellite Orbit satellites (IGSOs) and four Medium Earth Orbit satellites (MEOs). BDS-3 with 30 satellites will be established in 2020, and China implemented the BDS-3 experimental project in order to demonstrate the new generation of BDS from 2015 to 2016. Compared to BDS-2, the User Equivalent Range Error (UERE) is reduced, the multipath effects have been weaken, and the estimation and prediction of satellite orbit, satellite clock offset have been greatly improved through support of the inter-satellite links [5]. Undoubtedly, the availability, reliability integrity, positioning accuracy and convergence speed of the GPS/BDS RTK, and even the multiple-constellation GNSS RTK, can be significantly improved in comparison with the GPS alone RTK [6–8]. As a result, improving the performance of GPS alone RTK and GPS/BDS RTK over the medium- and long-range baselines will be the main focus of this study.

In GNSS positioning, the main errors can be grouped as three parts: satellite-related errors, propagation-related errors and receiver-related errors. Satellite-related errors, such as satellite clock error, orbit error, and wind-up effect, are very similar to receivers, and they can be removed or reduced by differential methods or using International GNSS Service (IGS) real-time product. Receiver related error sources include receiver clock errors, measurement noise and multipath. These errors are local environmental dependent, and cannot be removed by external augmentations. Fortunately, with the development of receiver technology, the accuracy of pseudorange is approaching 10 cm or less; carrier phase can achieve millimeter accuracy. Propagation-related effect is introduced by the troposphere and ionosphere when GPS signals traverse from the satellite to the receiver. As GNSS are providing triple-even multiple-frequency signals, ionospheric delays can be removed from the combinations of different frequencies [8–10]. As was reported in our paper [11], we developed a new ionosphere-free ambiguity resolution method for long-range baselines, which can eliminate the ionospheric delay in the ambiguity search stage. Different from the ionosphere, the troposphere is a non-dispersive medium and includes hydrostatic (dry) delay and non-hydrostatic or wet delay [12]. The hydrostatic delay typically reaches about 2.3 m in the zenith direction at sea level [13] and can be accurately modeled [14,15]. Although the wet part only contributes about 10% of the total tropospheric delay, it is very difficult to model adequately using only surface measurements. The accuracy of conventional wet delay models, i.e., the Hopfield model, Ifadis model [16] and Meddes model [17], can be over 5 cm vertically, which can cause positioning errors of more than 1.5 m [18]. Double difference can be used to reduce the tropospheric delay, but it is not suitable for the long-range baseline RTK. High-precision tropospheric delay can also be estimated by GNSS carrier-phase measurements, together with position, ionospheric delay, and ambiguity [19,20]. This technique has been widely used for water vapor estimation and high-precision differential positioning [21]. However, this method requires a period of time for the accurate estimation of the tropospheric delay parameters. Another method to eliminate the effect of wet tropospheric delay is to measure it directly with instruments: radiosonde, infrared spectral hygrometer and water vapor radiometer (WVR). WVR is the most commonly used instrument, and its accuracy can reach about 1 cm [22]. However, the cost of these instruments is too high to install

them at each reference and rover station. As a result, tropospheric delay is the most significant error that affects the performance of the RTK, especially over the long-rang RTK.

Apart from the methods mentioned above, the numerical weather prediction (NWP) model can also be used to estimate the tropospheric delay. The meteorological parameters can be derived at any location and at any time within the area by using the required information from NWP models for describing the neutral atmosphere. Using these meteorological parameters, tropospheric delays of the area can be estimated. Many researchers have applied zenith tropospheric delay (ZTD) measured by GPS to validate the ZTD derived from meteorological data and concluded that they basically agreed with each other [23–26]. Research demonstrated that the ZTD derived from the NWP model-global data acquisition system (GDAS) agreed with the IGS ZTD solutions at a 3.0 cm root mean square difference (RMSD) level with biases of up to 4.5 cm over a 1.5-year period at 18 globally distributed IGS stations [27]. The test results of [28] showed that the RMSD of the ZTD calculated by the European Centre for Medium-Range Weather Forecasts (ECMWF), reanalyzed data with a horizontal resolution of $0.5^\circ \times 0.5^\circ$ in China, was 3.54 cm and that of the National Centers for Environmental Prediction (NCEP), with a horizontal resolution of $2.5^\circ \times 2.5^\circ$, was 5.36 cm. However, the tropospheric delay estimated by the reanalyzed data cannot be used in real-time positioning. Experimental results showed that the RMSD of the ZTD derived from NCEP surface forecast data was 10 cm over China [28]. Research also demonstrated that although independent observation showed good accuracy of the zenith hydrostatic delay (ZHD) derived from the NWP models, the accuracy of the zenith wet delay (ZWD) derived from these models was usually far less than that of the ZHD, especially in low-altitude regions [29]. A few studies have been done to investigate the possible use of ray-tracing using raw NWP models to improve GPS RTK processing [30–33]. The effectiveness of the network RTK initialization was improved by 19% using the National Oceanic and Atmospheric Administration (NOAA) model compared with the Hopfield model [30]. Although an improvement of about 60% in the vertical coordinate bias was found, the absolute accuracy cannot be expected to be better than 10 cm owing to the remaining mis-modeling of the troposphere [31]. As a result, the ZTD derived from NWP models is still not accurate enough for high-precision GNSS real time positioning applications without the estimation of the residual tropospheric delay.

In this study, we focus on developing and testing a new GPS/BDS RTK processing algorithm constrained with the NWP model to improve the GPS/BDS double difference precise positioning over medium/long-range baselines. Tropospheric delay parameters, which are derived from the medium-range NWP model from the Shanghai Meteorological Bureau (SMB), are applied to GPS/BDS RTK. The precise tropospheric delay is computed using GPS observation with GAMIT (GNSS at MIT) software, which is one of the most famous GPS precise data processing software packages [34]. The quality of tropospheric delay parameters retrieved from this medium-range NWP model is assessed by comparison with the result of GAMIT. The performance of GPS RTK and GPS/BDS RTK making use of the NWP-derived tropospheric delay parameters is evaluated in terms of both initialization time and positioning accuracy.

Descriptions for multiple-GNSS and the tropospheric delay estimation methods are presented in the "Introduction" section. In this section, we also investigate the significance and challenge of estimating the tropospheric delay using the NWP model. The NWP data collection and theoretical foundation of the new RTK algorithm constrained with the NWP model proposed in this study can be found in "Materials and Methods" section. The quality of the tropospheric delay derived from the NWP model used in this study is assessed in "Results" section. To examine the performance of the NWP-constrained RTK, compared with that of the standard RTK, experiments are carried out based on GPS and BDS observation over medium/long-range baselines. Finally, a discussion and conclusions are presented based on our findings.

2. Materials and Methods

2.1. Data Collection

In this study, the pressure, temperature, and specific humidity fields of the medium-range NWP model from the SMB are utilized to retrieve the tropospheric delay parameters. This model is established based on the Weather Research and Forecasting Model (WRF). It covers the East China area, and it includes three types of spatial resolutions: 3 km, 9 km and 15 km. The horizontal resolution of 9 km with 35 vertical levels is used for this study. The exponential model is used for the tropospheric correction up to the 50 hPa. The temporal resolution of the NWP in this study is 3 h. In addition, one year's NWP data over the East China area and GNSS observations of eight meteorological stations (BYFH, BTLU, BTUZ, BXTC, ZJHZ, SDHM, SDJM, SHBS) in eastern China were collected to validate the ZTD derived from NWP. The eight stations shown in Figure 1 are located between Latitude 28°N and 38°N, Longitude 116°E and 122°E.

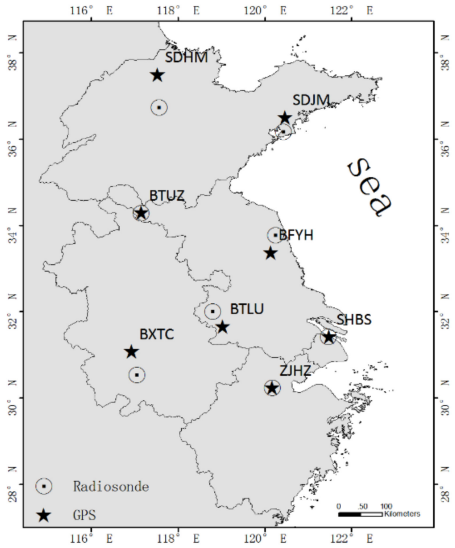

Figure 1. Distribution map of the experimental stations.

2.2. NWP ZTD Integral Method

Two methods: the integral method and model estimation method, are commonly used to derive the ZTD from the NWP meteorological parameters [28]. In this study, the results of the integral method and model estimation method was compared by computing the tropospheric delay of one reference station for one year using these two methods. Treating the tropospheric delay gained by GAMIT as the precise value, the tropospheric delay residual of the two methods are shown in Figure 2. From this figure, we can see the residual of the integral method generally vary between ±40 mm, while the residual of the model estimation method can reach ±60 mm. The standard deviation of the tropospheric delay residual of the integral method is 17.5 mm, and is 33.2 mm for the model estimation method. As a result, the accuracy of the tropospheric delay from the integral method is better than the model estimation method in this experiment. Although the integral method gets a better results in this experiment, we also agree that the accuracy depends on the level of integration.

The integral method is applied in this study. The physical conditions on each 3D grid point of NWP products (e.g., pressure, temperature, relative humidity, and height) are used to calculate the atmospheric refractivity N of each grid point (Equation (1)), and the ZTD is estimated by the integral method using Equation (2).

$$N = k_1 \frac{(P-e)}{T} + \left(k_2 \frac{e}{T} + k_3 \frac{e}{T^2}\right) = N_{\text{dry}} + N_{\text{wet}} \quad (1)$$

$$\mathrm{ZTD} = 10^{-6} \sum_{\mathrm{i}=1}^{n} N_i \Delta \mathrm{H}_i \tag{2}$$

where $k_1 = 77.6890$ K/mbar, $\mathrm{k}_2 = 71.2952$ K/mbar, and $k_3 = 375{,}463$ K^2/mbar are empirically determined coefficients [35], T is the temperature (unit: K), P and e are atmospheric pressure and water vapor pressure (unit: mbar), N_{dry} and N_{wet} are the refractivity of dry gas and refractivity of wet gas, N_i is the atmospheric refractivity in the i th integral area (it equals the average of two adjacent layers' grid points), $\Delta \mathrm{H}_i$ is the height of the i th integral area, and n is the level of integration, which depends on the number of levels of meteorological data from the observation station to the top of the meteorological data.

Since the observation station would not be located at the grid points, the ZTD of the observation station are obtained using bilinear interpolation (horizontal direction) and the Gaussian function model (vertical direction) in this study [36].

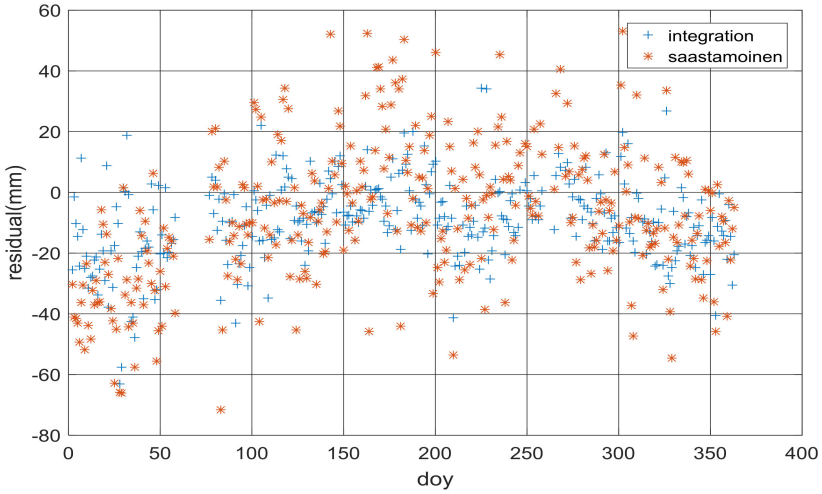

Figure 2. Tropospheric delay residual of the integral method and model estimation method.

2.3. GPS/BDS Medium/Long-Range RTK Algorithm Constrained with NWP Model

In long-range baselines RTK, measurement errors (tropospheric delay, ionospheric delay, relativistic effects, solid earth tides, polar tides and ocean loading tides) should be considered. The tides and other geophysical related errors can be estimated using methods and models. As a consequence, the main errors that affect the performance of GPS/BDS RTK are the tropospheric delay and ionospheric delay. In this study, we focus on the tropospheric delay, and use the ionospheric delay estimation method for medium/long-range baselines we developed to reduce the ionospheric delay [11]. After the ionospheric delay and other measurement errors are removed, the GPS/BDS RTK processing model can be expressed as follows:

$$\begin{bmatrix} v_{\Delta P_{Gi}} \\ v_{\Delta \varphi_{Gi}} \\ v_{\Delta P_{Bj}} \\ v_{\Delta \varphi_{Bj}} \end{bmatrix} = \begin{bmatrix} A & C & 0 & 0 \\ A & C & \lambda_{Gi} \cdot E & 0 \\ A & C & 0 & 0 \\ A & C & 0 & \lambda_{Bj} \cdot E \end{bmatrix} \begin{bmatrix} B \\ T \\ \Delta N_{Gi} \\ \Delta N_{Bj} \end{bmatrix} - \begin{bmatrix} \Delta P_{Gi} \\ \Delta \varphi_{Gi} \\ \Delta P_{Bj} \\ \Delta \varphi_{Bj} \end{bmatrix} \tag{3}$$

where $v_{\Delta P_{Gi}}$ and $v_{\Delta \varphi_{Gi}}$ are the residual vectors of the double difference GPS pseudo-range and phase observation; $v_{\Delta P_{Bj}}$ and $v_{\Delta \varphi_{Bj}}$ are the residual vectors of the double difference BDS pseudo-range and phase observation; i, j denote the frequency; A is the design matrix; C is the coefficient corresponding to T; λ_{Gi} and λ_{Bj} are the wavelength of the corresponding GPS and BDS observation, respectively; E is the unit matrix; B, T are the vectors of unknown parameters of baseline components and double difference slant total delay,

respectively; ΔN_{Gi} and ΔN_{Bj} are the GPS and BDS double difference ambiguity, respectively; ΔP_{Gi}, $\Delta \varphi_{Gi}$, ΔP_{Bj} and $\Delta \varphi_{Bj}$ are the double difference GPS and BDS pseudo-range and phase observation, respectively.

The double difference slant total delay T can be described as the sum of the double difference hydrostatic and non-hydrostatic orwet components [12]:

$$\Delta \mathrm{T} = \Delta_{\mathrm{ZHD}} \cdot \mathrm{mfh} + \Delta_{\mathrm{ZWD}} \cdot \mathrm{mfnh} \tag{4}$$

where Δ_{ZHD} and Δ_{ZWD} denote the double difference zenith hydrostatic and double difference non-hydrostatic orwet delays, respectively; mfh and mfnh are the double difference hydrostatic and non-hydrostatic mapping functions, respectively; and we used the GMF Global Mapping Function (GMF) in this research [37].

In this study, four RTK scenarios are applied concerning the approach for tropospheric delay modeling and GPS/BDS integration positioning: the standard RTK (GPS alone), the standard GPS/BDS RTK, the RTK constrained with NWP (GPS alone) and the GPS/BDS RTK constrained with NWP ZTD. For the standard RTK processing (both GPS alone and GPS/BDS RTK), the Δ_{ZHD} is calculated by using the Hopfield model in this study [14]. Owing to the high variability of the water vapor distribution, the Δ_{ZWD} is estimated as an unknown parameter in the adjustment together with the other parameters, such as the station coordinates and the ambiguities. All of the unknown parameters are adjusted in a sequential least squares filter. For the standard RTK processing, the unknown parameter vector X can be described as

$$\mathrm{X} = \left(\mathrm{B}\Delta_{\mathrm{ZWD}}\Delta\mathrm{N}_{\mathrm{Gi}}\Delta\mathrm{N}_{\mathrm{Bj}}\right)^{T} \tag{5}$$

As with the standard RTK, we remove the Δ_{ZHD} firstly in the NWP-constrained RTK (both GPS alone and GPS/BDS RTK). In a different way from the standard RTK, the priori Δ_{ZWD} predicted by the NWP model with a prior variance of the wet troposphere parameters is introduced to the troposphere vector in this algorithm. At the same time, a wet delay residual $\mathrm{Resi}_{\Delta_{\mathrm{ZWD}}}$ is estimated as an unknown parameter during the processing in order to account for possible imperfections inherent in the NWP. The constraints of the residual Δ_{ZWD} are referred to as the prior variance, and the definition of this prior variance will be proposed in the next section. The unknown parameter vector X in the NWM-constrained RTK can be expressed as

$$\mathrm{X} = \left(\mathrm{B}\mathrm{Resi}_{\Delta_{\mathrm{ZWD}}}\Delta\mathrm{N}_{\mathrm{Gi}}\Delta\mathrm{N}_{\mathrm{Bj}}\right)^{T} \tag{6}$$

where $\mathrm{Resi}_{\Delta_{\mathrm{ZWD}}}$ is the wet delay residual.

Comparing the RTK algorithms, they have the same number of unknown troposphere parameters. However, the NWP-constrained RTK applies the external meteorological information and the prior variance information. The RTK performance of this algorithm would be better in theory, if the priori Δ_{ZWD} predicted by NWP model has high accuracy.

3. Results

3.1. Tropospheric Delay Comparison between NWP and GAMIT

Different regional NWP models may have different accuracy and therefore detailed evaluations are required to assess the accuracy of different models. In this study, the NWP model we used is the main medium-range NWP model from the SMB. To investigate the quality of ZTD parameters derived from the NWP model, we compare the value of the tropospheric delay calculated by NWP and GAMIT. To achieve this objective, one year's NWP data over East China area and GNSS observation on eight meteorological stations in Figure 1 were collected. The tropospheric delays of these eight stations were calculated with GAMIT every 1 h. As the NWP ZTD are sampled every 3 h, we do not interpolate in time but restrict the comparison to the NWP data epochs.

As typical examples, the ZTD series derived from the medium-range NWP model and GAMIT at stations BXTC, SDJM and SHBS are shown in Figures 3–5. From these figures, we can see the time series of the NWP ZTD are in relatively good agreement with GAMIT ZTD. The correlation coefficient showed in Table 1 are all larger than 0.97, which also suggest that these two kinds of ZTD are highly correlated. Generally, the peaks of these ZTD series appear between the 180th and 210th day of year, which are during the rainy season. As a result, rapid and large changes of water vapor would increase the variability of tropospheric delay. Taking the tropospheric delay gained from GAMIT as the precise value, the residuals of the estimation using the NWP method are shown in Figure 6. Table 1 presents the average values and the Root Mean Square error (RMS) of the residuals during the experimental period. From Figure 6, we can see the maximum and minimum values of the residuals are about 200 mm and −150 mm, and the NWP ZTD residuals are mainly distributed between −50 mm and 50 mm. The mean residuals are between −5.50 and 5.60 mm, and the RMS are between 24.02 and 32.62 mm (Table 1). The station of BTLU shares the best precision, while the RMS of station SHBS, SDJM and ZJHZ are relatively large. In this study, we set the mean value of the RMS of these eight stations as the prior variance of tropospheric delay residuals for the stations in this area.

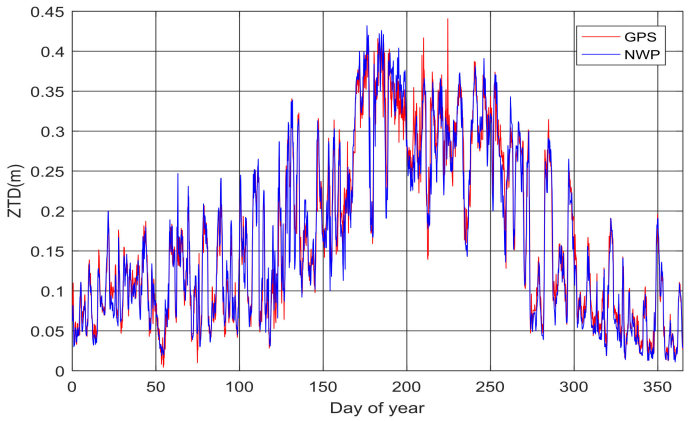

Figure 3. Time series of NWP ZTD (blue line) and GAMIT ZTD (red line) at station BXTC.

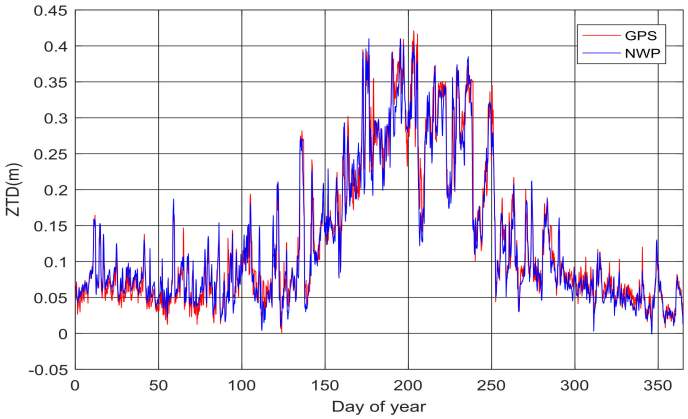

Figure 4. Time series of NWP ZTD (blue line) and GAMIT ZTD (red line) at station SDJM.

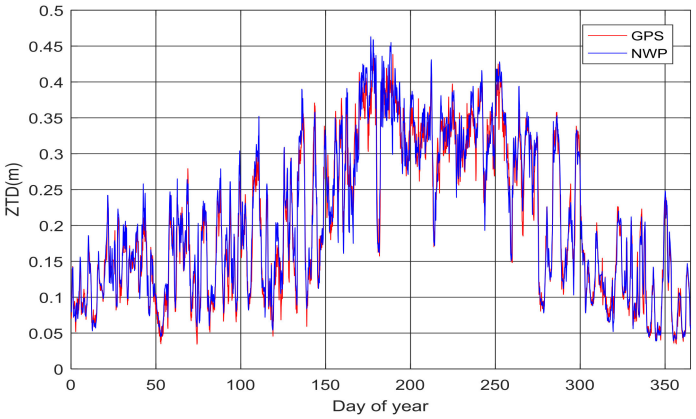

Figure 5. Time series of NWP ZTD (blue line) and GAMIT ZTD (red line) at station SHBS.

Table 1. Mean residual, RMS and the correlation coefficients (CC) of NWP ZTD.

Station	BTLU	BFYH	BTUZ	BXTC	SDHM	ZJHZ	SDJM	SHBS
Mean (mm)	−4.10	−0.47	−5.34	3.17	5.60	−3.65	0.45	−5.50
RMS (mm)	24.02	24.08	24.47	25.08	27.63	28.10	28.22	32.62
CC	0.978	0.976	0.978	0.977	0.979	0.980	0.976	0.970

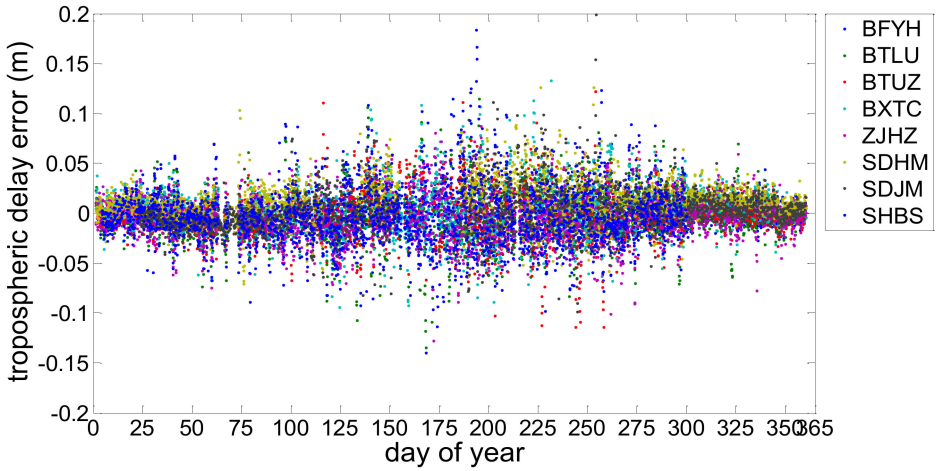

Figure 6. Tropospheric delay residuals of the experimental stations.

3.2. GPS/BDS RTK Results

To investigate the performance of the GPS/BDS RTK constrained with the ZTD derived from the medium-range NWP model, 10 days of GPS/BDS observations from three stations located in the medium-range NWP model covered area were collected. The observation interval was 1 s. The Trimble NetR9 receiver and TRM59800.00 antenna was used on these stations. Dual-frequency code and carrier phase signals of GPS (L1, L2) and BDS (B1, B2) were used in this experiment. In this experimental period, two baselines between the stations were studied and the lengths of the baselines were about 80 and 260 km, respectively. GPS/BDS observation was processed every minute using four schemes following the data processing algorithms presented in Section 2 until the corresponding ambiguity validation conditions were satisfied. The four schemes were the standard GPS RTK, standard GPS/BDS RTK, GPS RTK constrained with NWP ZTD and GPS/BDS RTK constrained with NWP ZTD. In the data processing, we mitigated the ionospheric delay using the medium/long-range baselines ionospheric

delay estimation method we developed [11]. The popular R-ratio [38] was used as the validation method and a threshold value was set to 2.5. For composing the weight matrix, the sigma of carrier phase noise was set to 3 mm for both GPS and BDS. Before setting the sigma of the code measurements of BDS and GPS, we assess the multipath and code noise level using the multipath combination (MPC). The combination is constructed using a single-frequency code measurement and dual-frequency phase measurements, which can be expressed as:

$$\mathrm{MP1} = P_1 - \frac{f_1^2+f_2^2}{f_1^2-f_2^2}\phi_1 + \frac{2f_2^2}{f_1^2-f_2^2}\phi_2 \quad (7)$$

$$\mathrm{MP2} = P_2 - \frac{2f_1^2}{f_1^2-f_2^2}\phi_1 + \frac{f_1^2+f_2^2}{f_1^2-f_2^2}\phi_2 \quad (8)$$

where P_i and ϕ_i $(i = 1, 2)$ are the GNSS code and carrier phase measurements, respectively; and f_i denotes the frequency for carrier phase.

One day of GPS/BDS dual-frequency observations from one station located in the medium-range NWP model covered area were collected for this experiment. Table 2 shows the standard deviations of BDS MPCs. The standard deviations vary in a range of 0.200–0.577 m. The average of all standard deviations for B1 MPCs is 0.318 m, which is larger than that of GPS L1 codes (0.243 m). While for B2 MPCs, the average of standard deviations is 0.385 m, which is also larger than that of GPS L2 codes (0.297 m). Experimental results show that the multipath and noise level of BDS code measurements is higher than that of GPS collected using the same receiver. However, it should be mentioned that it is not completely fair to compare MPCs of BDS and GPS satellites as the constellations of two GNSS system are completely different. As the multipath and code noise level of BDS pseudo-range measurements was larger than that of GPS, the sigma of pseudo-range noise was set to 0.5 m for BDS, instead of 0.3 m for GPS [11].

Table 2. The standard deviations of multipath combinations for BDS satellites (unit: m).

	C01	**C02**	**C03**	**C04**	**C05**
MP1	0.200	0.210	0.231	0.277	0.263
MP2	0.223	0.232	0.244	0.309	0.301
	C06	C07	C08	C09	C10
MP1	0.433	0.411	0.306	0.316	0.278
MP2	0.381	0.392	0.371	0.382	0.384
	C11	C12	C13	C14	
MP1	0.366	0.432	0.356	0.367	
MP2	0.502	0.577	0.519	0.511	

Time required for AR or initialization is an important index to measure the performance of the RTK and the benefit of the NWP ZTD. Figures 7 and 8 show the time needed to fix the ambiguities using the data processing algorithms mentioned above. Table 3 presents the mean times for AR and the improvement of NWP-constrained RTK, with respect to the standard RTK for both GPS/BDS and GPS alone solutions. For the baseline of 80 km, it is noted that about 40% of ambiguities are fixed in 20 min with standard GPS RTK, while over 77% of initialization can be achieved in 20 min with standard GPS/BDS RTK. The mean time needed is reduced by 31.0% when BDS is involved. GPS RTK constrained with NWP ZTD only need a mean time of 13.3 min for initialization and this can be improved by 41.2%, compared with the standard GPS RTK. Over 90% of ambiguities can be fixed in 15 min by using the process scheme of GPS/BDS RTK constrained with NWP ZTD. The mean time needed (8.8 min) is also improved by 43.6% comparing with the standard GPS/BDS RTK. For the

baseline of 260 km, the initialization required time is about twice as much as that of the baseline of 80 km. The mean time of 49.7 min is needed for obtaining the fixed solution with standard GPS RTK. In comparison, it takes about 20 min (mean time) for the AR with the GPS RTK constrained with NWP ZTD, shortening the solution initialization time by 58.8%. Similarly, a significant reduction of 62.7% is revealed by the GPS/BDS RTK constrained with NWP ZTD compared with the standard GPS/BDS RTK. The mean time needed is only 12.9 min. In addition, an improvement 30% or more can be found in the initialization time when BDS is involved in RTK for both the standard and NWP-constrained mode solutions. As a result, firstly, the initialization speed can be remarkably improved with the GPS/BDS solutions, compared with that of the GPS RTK for both medium- and long-range baselines. Secondly, the NWP-constrained RTK reveals significant contribution to improving the initialization speed of both GPS and GPS/BDS solutions.

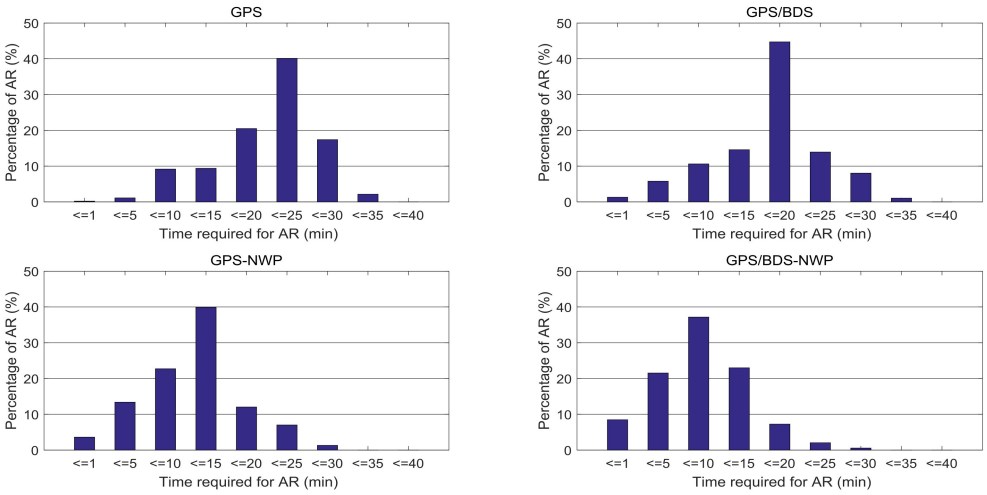

Figure 7. Time required for AR (baseline: 80 km).

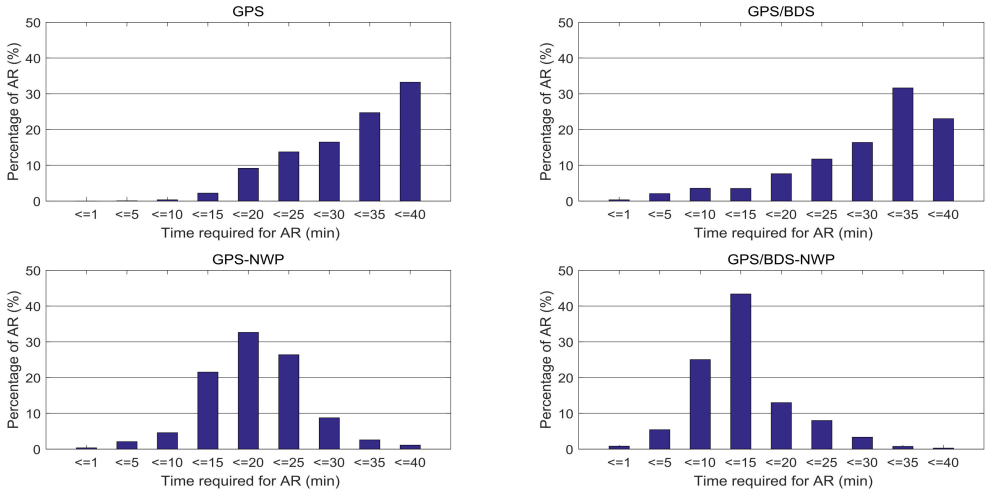

Figure 8. Time required for AR (baseline: 260 km).

Table 3. Mean times for AR and the improvement of NWP-Constrained RTK (NWP-RTK) respecting to the standard RTK for both GPS/BDS and GPS Solutions.

		GPS	GPS/BDS	Improvement
Baseline 80 km	Standard RTK	22.6 (min)	15.6 (min)	31.0%
	NWP-RTK	13.3 (min)	8.8 (min)	33.8%
	Improvement	41.2%	43.6%	
Baseline 260 km	Standard RTK	49.7 (min)	34.6 (min)	30.4%
	NWP-RTK	20.5 (min)	12.9 (min)	37.1%
	Improvement	58.8%	62.7%	

Another important index to measure the performance of the RTK is the positioning precision. Figures 9 and 10 illustrate the positioning error compared to the precise position. Since the experimental stations are continuously operating reference stations, the precise position of them are known. Table 4 shows the positioning precision (the standard deviation of the positioning error) of the baseline of 80 and 260 km in terms of the North, East and Up direction. Since the positioning precision of GPS/BDS RTK constrained with NWP is very similar to that of the other three RTK schemes mentioned above after the ambiguities are fixed successfully, we only display of the results of the NWP-constrained GPS/BDS RTK. From these figures and table, we can see the positioning precision is better than 3 cm in the horizontal direction and better than 5 cm in the vertical direction, which satisfies the requirement of the precise positioning service. The positioning error of the medium-range baseline (80 km) in the North and East direction floats between -0.02 m and $+0.02$ m, which increases to ± 0.04 m for the long-range baseline (260 km). Similarly, the positioning error in the direction of Up over long-range baseline is also lager than that over the medium-range baseline. Moreover, the standard deviation of the long-range baseline (260 km) is about twice as large as that of the medium-range baseline.

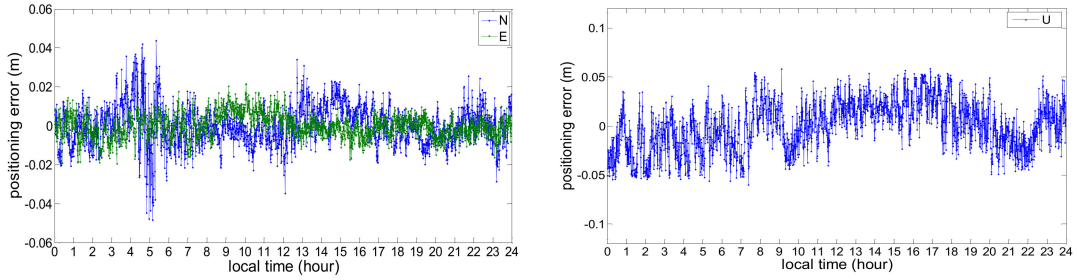

Figure 9. Positioning error of the North, East and Up direction (baseline: 80 km).

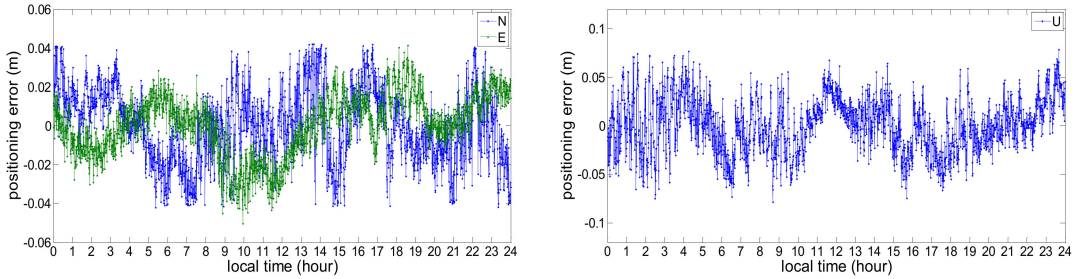

Figure 10. Positioning error of the North, East and Up direction (baseline: 260 km).

Table 4. Positioning Precision of the North, East and Up Direction (m).

Baseline	N	E	U
baseline: 80 km	0.013	0.010	0.026
baseline: 260 km	0.023	0.021	0.043

4. Discussion

To assess the accuracy of the tropospheric delay from the NWP and define the prior variance of the NWP ZTD, we compute the RMS of NWP ZTD residuals for eight stations. Experiments show that RMS of the tropospheric delay residuals derived from the medium-range NWP model from the SMB are between 24.02 and 32.62 mm, which is much better than that of the ECMWF and NCEP shown in the research of Chen et al. [28]. However, it should be mentioned that it is not completely fair to compare the ZTD residual of them as the spatial resolutions of them are different. Research has shown that the RMS values of the tropospheric delay residual from the NWP revealed strong dependence on geographical latitudes: smaller in high-latitude and larger in low latitude areas [31]. In this condition, the prior variance of the NWP ZTD error is set considering the latitude of the stations. However, the ZTD from the medium-range NWP model in this study doesn't show this characteristic due to the limited area size. As a result, we set the mean value of the RMS of these eight stations as the prior variance of tropospheric delay error for the stations in this area.

Experimental results (Figures 7 and 8 and Table 3) in our study show that the initialization speed improvement of NWP-constrained RTK for the long-range baseline is larger than that of the medium-range baseline. The possible reason would be that the tropospheric delay is one kind of distanced based error, which would be canceled through double difference over the medium-range baseline. However, the effectiveness of double difference will be weakened substantially for the long-range baseline due to the weak spatial correlation, and the residuals of the tropospheric delay after double difference over long-range baseline are declined by using the NWP model significantly.

In our study, although the positioning precise of the GPS/BDS RTK constrained with NWP is satisfactory, the positioning precise of the long-range baseline is worse than that of the medium-range baseline. Larger error also results in a longer time needed for the AR over the long-range baseline shown in Table 3. The possible reasons would be: (1) most of the errors (solid earth tides, polar tides, ocean loading tides, etc.), which can be ignored in the medium-range baseline, should be estimated in the long-range baselines. However, the residuals of these errors after modeling or estimation will definitely affect the positioning precision; (2) the accuracy of the ZTD from the NWP model and the prior variance information for the ZTD residuals is not high enough. Both of the possible reasons remain to be further studied.

5. Conclusions

In this study, we developed a new GPS/BDS medium/long-range RTK algorithm constrained with tropospheric delay parameters from the medium-range NWP model. One year's NWP data over East China area and GPS/BDS observation of eight stations were processed. The accuracy of the tropospheric delays derived from NWP was assessed through comparisons with the results of GAMIT at these stations. The positioning performance with standard GPS RTK, standard GPS/BDS RTK, the developed NWP-constrained GPS RTK and NWP-constrained GPS/BDS RTK over medium- to long-range baselines were compared in terms of the initialization time and the positioning accuracy. The benefits of applying tropospheric delay parameters from the NWP model to improve the performance of GPS/BDS RTK were demonstrated. Experimental results show that,

(1) The mean difference between the NWP and GAMIT ZTD are between −5.50 mm and 5.60 mm, and the RMS values of the NWP ZTD residuals are from 24.02 to 32.62 mm. The tropospheric

delay from NWP can not be used in the RTK positioning directly without the estimation of the residual tropospheric delay.

(2) Most of the peaks of the NWP ZTD series appear in the rainy season, and the rapid and large change of water vapor would increase the variability of tropospheric delay. The ZTD from the medium-range NWP model in this study doesn't show the latitude based characteristics due to the limited area size.

(3) For the medium-range baseline (80 km), the NWP-constrained RTK (both GPS alone and GPS/BDS RTK solutions) show a reduction of over 41% in the initialization time compared with the standard RTK. This reduction for the long-range baseline (260 km) is over 58%.

(4) An improvement of over 30% in the initialization time can be achieved with the GPS/BDS RTK, compared with that of the GPS RTK for both standard and the NWP-constrained RTK modes.

(5) The positioning precision of NWP-constrained GPS/BDS RTK is better than 3 cm in horizontal direction and better than 5 cm in vertical direction, which satisfies the requirement of the precise positioning service.

Author Contributions: Y.X. and W.C. conceived and designed the experiments; M.L. provided the NWP data. Y.X., L.L. and L.Y. performed the experiments, analyzed the data and wrote the paper; W.C., S.W. and L.L. helped drew the pictures and modify the paper.

Funding: This work is supported by the National Natural Science Foundation of China (41704021), the Natural Science Foundation of Shandong Province of China (ZR2017QD002), the Scientific Research Foundation of Shandong University of Science and Technology for Recruited Talents (2017RCJJ075).

Conflicts of Interest: The authors declare no conflict of interest.

References

1. Zumberge, J.F.; Heflin, M.B.; Jefferson, D.C.; Watkins, M.M.; Webb, F.H. Precise point positioning for the efficient and robust analysis of GPS data from large networks. *J. Geophys. Res. Solid Earth* **1997**, *102*, 5005–5017. [CrossRef]
2. Bisnath, S.; Gao, Y. *Current State of Precise Point Positioning and Future Prospects and Limitations*; Springer: Berlin/Heidelberg, Germany, 2008; pp. 615–623.
3. Han, S. Carrier Phase-Based Long-Range GPS Kinematic Positioning. Ph.D. Thesis, UNSW University, Sydney, Australia, 1997.
4. Teunissen, P.J.G.; Odijk, D. Rank-defect integer estimation and phase-only modernized GPS ambiguity resolution. *J. Geod.* **2003**, *76*, 523–535. [CrossRef]
5. Yang, Y.; Xu, Y. *Performance Analysis of Experimental System of BDS-3*; ISGNSS: Hong Kong, China, 2017.
6. Liang, X.; Huang, Z.; Qin, H.; Liu, Y. GNSS multi-frequency multi-system highly robust differential positioning based on an autonomous fault detection and exclusion method. *IEEE Access* **2017**, *5*, 26842–26851. [CrossRef]
7. He, H.; Li, J.; Yang, Y.; Xu, J.; Guo, H.; Wang, A. Performance assessment of single-and dual-frequency BeiDou/GPS single-epoch kinematic positioning. *GPS Solut.* **2014**, *18*, 393–403. [CrossRef]
8. Ji, S.; Chen, W.; Ding, X.; Chen, Y.; Zhao, C. Potential benefits of GPS/GLONASS/GALILEO integration in an urban canyon–Hong Kong. *J. Navig.* **2010**, *63*, 681–693. [CrossRef]
9. Feng, Y.; Li, B. A benefit of multiple carrier GNSS signals: Regional scale network-based RTK with doubled inter-station distances. *J. Spat. Sci.* **2009**, *53*, 135–147. [CrossRef]
10. Li, B.; Feng, Y.; Shen, Y. Three carrier ambiguity resolution: Distance-independent performance demonstrated using semi-generated triple frequency GPS signals. *GPS Solut.* **2009**, *14*, 177–184. [CrossRef]
11. Xu, Y.; Ji, S.; Chen, W.; Weng, D. A new ionosphere-free ambiguity resolution method for long-range baseline with GNSS triple-frequency signals. *Adv. Space Res.* **2015**, *56*, 1600–1612. [CrossRef]
12. Chen, G.; Herring, T.A. Effects of atmospheric azimuth asymmetry on the analysis of space geodetic data. *J. Geophys. Res.* **1997**, *102*, 20489–20502. [CrossRef]
13. Schüler, T. *On Ground-Based GPS Tropospheric Delay Estimation*; University der Bundeswehr München: Neubiberg, Germany, 2001.

14. Hopfield, H.S. Two-quartic tropospheric refractivity profile for correcting satellite data. *J. Geophys. Res.* **1969**, *74*, 4487–4499. [CrossRef]
15. Saastamoinen, J. Contributions to the theory of atmospheric refraction. *Bull. Géod. (1946–1975).* **1972**, *107*, 13–34. [CrossRef]
16. Ifadis, I. *The Atmospheric Delay of Radio Waves: Modeling the Elevation Dependence on a Global Scale*; Technical Report No. 38L; School of Electrical and Computer Engineering, Chalmers University of Technology: Gothenburg, Sweden, 1986.
17. Mendes, V.B.; Langley, R.B. Tropospheric zenith delay prediction accuracy for airborne GPS high-precision positioning. In Proceedings of the Annual Meeting of the Institute of Navigation 54th Annual Meeting, Denver, CO, USA, 1–3 June 1998; Volume 23, pp. 171–174.
18. Penna, N.; Dodson, A.; Chen, W. Assessment of EGNOS tropospheric correction model. *J. Navig.* **2001**, *54*, 37–55. [CrossRef]
19. Lu, C.; Chen, X.; Liu, G.; Dick, G.; Wickert, J.; Jiang, X.; Zheng, K.; Schuh, H. Real-time tropospheric delays retrieved from multi-GNSS observations and IGS real-time product streams. *Remote Sens.* **2017**, *9*, 1317. [CrossRef]
20. Lu, C.; Li, X.; Cheng, J.; Dick, G.; Ge, M.; Wickert, J.; Schuh, H. Real-time tropospheric delay retrieval from multi-GNSS PPP ambiguity resolution: Validation with final troposphere products and a numerical weather model. *Remote Sens.* **2018**, *10*, 481. [CrossRef]
21. Jiang, P.; Ye, S.R.; Liu, Y.Y.; Zhang, J.J.; Xia, P.F. Near real-time water vapor tomography using ground-based GPS and meteorological data: Long-term experiment in Hong Kong. *Ann. Geophys.* **2014**, *32*, 911–923. [CrossRef]
22. Elgered, G.; Davis, J.L.; Herring, T.A.; Shapiro, I.I. Geodesy by radio interferometry: Water vapor radiometry for estimation of the wet delay. *J. Geophys. Res.* **1991**, *96*, 6541–6555. [CrossRef]
23. Vedel, H.; Mogensen, K.S.; Huang, X.Y. Calculation of zenith delays from meteorological data comparison of NWP model, radiosonde and GPS delays. *Phys. Chem. Earth* **2001**, *26*, 497–502. [CrossRef]
24. Song, S.; Zhu, W.; Ding, J.; Liao, X.; Cheng, Z. Near real-time sensing of PWV from SGCAN and the application test in numerical weather forecast. *Chin. J. Geophys.* **2004**, *47*, 719–727. [CrossRef]
25. Walpersdorf, A.; Bouin, M.N.; Bock, O.; Doerflinger, E. Assessment of GPS data for meteorological applications over Africa: Study of error sources and analysis of positioning accuracy. *J. Atmos. Sol.-Terr. Phys.* **2007**, *69*, 1312–1330. [CrossRef]
26. Liou, Y.A.; Teng, Y.T.; Van Hove, T.; Liljegren, J.C. Comparison of precipitable water observations in the near tropics by GPS, microwave radiometer, and radiosondes. *J. Appl. Meteorol.* **2001**, *40*, 5–15. [CrossRef]
27. Andrei, C.O.; Chen, R. Assessment of time-series of troposphere zenith delays derived from the global data assimilation system numerical weather model. *GPS Solut.* **2009**, *13*, 109–117. [CrossRef]
28. Chen, Q.; Song, S.; Heise, S.; Liou, Y.A.; Zhu, W.; Zhao, J. Assessment of ZTD derived from ECMWF/NCEP data with GPS ZTD over China. *GPS Solut.* **2011**, *15*, 415–425. [CrossRef]
29. Ghoddousi-Fard, R.; Dare, P. Comparing various GNSS neutral atmospheric delay mitigation strategies: A high latitude experiment. In Proceedings of the 19th International Technical Meeting of the Satellite Division of The Institute of Navigation (ION GNSS), Fort Worth, TX, USA, 26–29 September 2006; pp. 1945–1953.
30. Ahn, Y.W.; Lachapelle, G.; Skone, S.; Gutman, S.; Sahm, S. Analysis of GPS RTK performance using external NOAA tropospheric corrections integrated with a multiple reference station approach. *GPS Solut.* **2006**, *10*, 171–186. [CrossRef]
31. Cucurull, L.; Sedo, P.; Behrend, D.; Cardellach, E.; Rius, A. Integrating NWP products into the analysis of GPS observables. *Phys. Chem. Earth* **2002**, *27*, 377–383. [CrossRef]
32. Yang, L.; Hill, C.; Moore, T. Numerical weather modeling-based slant tropospheric delay estimation and its enhancement by GNSS data. *Geo-Spat. Inf. Sci.* **2013**, *16*, 186–200. [CrossRef]
33. Lu, C.; Zus, F.; Ge, M.; Heinkelmann, R.; Dick, G.; Wickert, J. Tropospheric delay parameters from numerical weather models for multi-GNSS precise positioning. *Atmos. Meas. Tech.* **2016**, *9*, 1–32. [CrossRef]
34. Kashani, I.; Wielgosz, P.; Grejnerbrzezinska, D.A. On the reliability of the VCV matrix: A case study based on GAMIT and Bernese GPS software. *GPS Solut.* **2004**, *8*, 193–199. [CrossRef]
35. Rüeger, J.M. *Refractive Index Formulae for Radio Waves*; International Congress: Washington, DC, USA, 2002.

36. Hu, Y.; Yao, Y. An Accurate Height Reduction Model for Zenith Tropospheric Delay Correction Using ECMWF Data. In Proceedings of the CSNC, Shanghai, China, 3 May 2017; pp. 337–348.
37. Boehm, J.; Niell, A.; Tregoning, P.; Schuh, H. Global Mapping Function (GMF): A new empirical mapping function based on numerical weather model data. *Geophys. Res. Lett.* **2006**, *33*. [CrossRef]
38. Teunissen, P.J.G.; Verhagen, S. The GNSS ambiguity ratio-test revisited: A better way of using it. *Surv. Rev.* **2009**, *41*, 138–151. [CrossRef]